

An Improved Snow Scheme for the ECMWF Land Surface Model: Description and Offline Validation

EMANUEL DUTRA,^{*,+} GIANPAOLO BALSAMO,[#] PEDRO VITERBO,[@] PEDRO M. A. MIRANDA,^{*}
ANTON BELJAARS,[#] CHRISTOPH SCHÄR,⁺ AND KELLY ELDER[&]

^{*} *Centro de Geofísica da Universidade de Lisboa, Instituto Dom Luiz, University of Lisbon, Lisbon, Portugal*

⁺ *Institute for Atmospheric and Climate Science, ETH, Zurich, Switzerland*

[#] *European Centre for Medium-Range Weather Forecasts, Reading, United Kingdom*

[@] *Institute of Meteorology, Lisbon, Portugal*

[&] *Rocky Mountain Research Station, USDA Forest Service, Fort Collins, Colorado*

(Manuscript received 3 December 2009, in final form 15 March 2010)

ABSTRACT

A new snow scheme for the European Centre for Medium-Range Weather Forecasts (ECMWF) land surface model has been tested and validated. The scheme includes a new parameterization of snow density, incorporating a liquid water reservoir, and revised formulations for the subgrid snow cover fraction and snow albedo. Offline validation (covering a wide range of spatial and temporal scales) includes simulations for several observation sites from the Snow Models Intercomparison Project-2 (SnowMIP2) and global simulations driven by the meteorological forcing from the Global Soil Wetness Project-2 (GSWP2) and by ECMWF Re-Analysis ERA-Interim. The new scheme reduces the end of season ablation biases from 10 to 2 days in open areas and from 21 to 13 days in forest areas. Global GSWP2 results are compared against basin-scale runoff and terrestrial water storage. The new snow density parameterization increases the snow thermal insulation, reducing soil freezing and leading to an improved hydrological cycle. Simulated snow cover fraction is compared against NOAA/National Environmental Satellite, Data, and Information Service (NESDIS) with a reduction of the negative bias of snow-covered area of the original snow scheme. The original snow scheme had a systematic negative bias in surface albedo when compared against Moderate Resolution Imaging Spectroradiometer (MODIS) remote sensing data. The new scheme reduces the albedo bias, consequently reducing the spatial- and time-averaged surface net shortwave radiation bias by 5.2 W m^{-2} in 14% of the Northern Hemisphere land. The new snow scheme described in this paper was introduced in the ECMWF operational forecast system in September 2009 (cycle 35R3).

1. Introduction

The extent and variability of snow cover are important parameters in weather and climate prediction systems because of their effects on energy and water balances, justifying a strong dependency of surface temperature on the presence or absence of snow cover (Armstrong and Brun 2008). Eurasian snow cover has been linked with the variability of the Indian summer monsoon (Douville and Royer 1996; Liu and Yanai 2002; Robock et al. 2003) and with significant changes in the hemispheric circulation (Cohen et al. 2007; Gong et al. 2007; Fletcher et al. 2009).

Snow cover also acts as a water reservoir, which is released by snowmelt in spring, influencing runoff, soil moisture, evaporation, and thus precipitation and the entire hydrological cycle (e.g., Douville et al. 2002; Groisman et al. 2004). Therefore, an accurate simulation of snow processes is essential for many applications ranging from hydrological forecast to numerical weather prediction (NWP), seasonal forecast, and climate modeling. Observed climate change during the twentieth century, particularly visible in the Northern Hemisphere surface warming in spring, has been significantly enhanced by the associated depletion of snow cover (Groisman et al. 1994a).

The presence of snow modulates the exchanges between the atmosphere and the surface. When compared with other natural surfaces, snow is remarkable in three different ways: an anomalously high albedo, an anomalously low thermal conductivity, and the ability to change

Corresponding author address: Emanuel Dutra, CGUL, IDL, Faculdade de Ciências Ed. C8, Campo Grande 1749-016 Lisbon, Portugal.
E-mail: endutra@gmail.com

phase (sometimes leading to coexisting liquid and solid water reservoirs). High surface albedo in the presence of snow causes rapid shifts in surface reflectivity in autumn and spring at high latitudes. Viterbo and Betts (1999) showed that changing the albedo of boreal forest in the presence of snow in the European Centre for Medium-Range Weather Forecasts (ECMWF) model reduced the model systematic cold bias at the surface at high northern latitudes in spring. Changes in the snow cover fraction and in its subgrid-scale variability are largely responsible for the observed interannual variability of surface albedo (Roesch and Roeckner 2006). On the other hand, the large amount of energy required to melt ice means that snow retards warming during the melting period. When melting occurs but is incomplete, liquid water may remain in the snowpack, significantly changing its properties and allowing for later refreezing. Because of that, the representation of a heterogeneous snowpack is important (Rutter et al. 2008), as are the effects of incident rainfall on the energy and mass balances (Bélair et al. 2003). The thermal insulation property of snow also has important climatic consequences. Cook et al. (2008) evaluated the impact of snow thermal conductivity in a climate model, reporting changes in soil temperature up to 20 K and in the air temperature up to 6 K during winter, just by prescribing snow thermal conductivity to its observed upper and lower limits. Grippa et al. (2005) showed that later snowmelt dates and thicker winter snowpacks are related to higher normalized difference vegetation index (NDVI) values over a large latitudinal band around 65°N. The authors suggested that this could be related to either an increased water availability for plants after snowmelt, or thermal insulation of the soil by snow.

The different treatment of snow processes in land surface models (LSMs) has been demonstrated in several offline LSM intercomparison experiments. The Tiled ECMWF Scheme of Surface Exchanges over Land (TESSEL) (a previous version of the model, but with the same snow scheme) participated in the Thorne–Kalix experiment (Nijssen et al. 2003; van den Hurk and Viterbo 2003), the Rhône Aggregation experiment (Boone et al. 2004), and the Snow Models Intercomparison Project-2 (SnowMIP2) (Essery et al. 2009; Rutter et al. 2009). Initial results of TESSEL in SnowMIP2 revealed some model weaknesses, such as early snowmelt in open sites and late melting in forest sites. These results motivated the development of the revised snow model described in the present paper.

Snow parameterizations in LSMs used in NWP, climate modeling, and in various applications such as hydrological forecasting or avalanche prediction vary greatly in complexity. Boone and Etchevers (2001) divided snow

schemes in three general categories according to their complexity: 1) simple force-restore or single explicit snow layer schemes (Verseghy 1991; Douville et al. 1995; Yang et al. 1997; Slater et al. 1998); 2) detailed internal-snow-process schemes (Anderson 1976; Brun et al. 1989; Jordan 1991); and 3) intermediate-complexity schemes based on class 2 but using simplified versions of the physical parameterizations (Loth et al. 1993; Lynch-Stieglitz 1994; Sun et al. 1999; Boone and Etchevers 2001). The Hydrology Tiled ECMWF Scheme of Surface Exchanges over Land (HTESSEL; Viterbo and Beljaars 1995; van den Hurk et al. 2000; Balsamo et al. 2009) included in the ECMWF model has a simple snow scheme, lying within the first category, with an explicit snow layer similar to the schemes described in Verseghy (1991) and Douville et al. (1995).

The present work describes a revision of HTESSEL's snow scheme and its validation. The snow scheme revision includes four main processes: 1) representation of liquid water content as a diagnostic, following a similar approach applied to soil phase changes by Viterbo et al. (1999); 2) new snow density parameterization following Anderson (1976) and Boone and Etchevers (2001); 3) revised snow cover fraction; and 4) revision of exposed snow albedo and new forest albedo in the presence of snow adapted from Moody et al. (2007). When compared to the original snow scheme three main differences can be identified: (i) dry versus wet snow in new scheme, (ii) simple exponential increase of snow density against a more physically based formulation in the new scheme, and (iii) constant forest albedo in the present of snow against a vegetation cover type dependence based on observations in the new scheme. The changes to the model (section 2) were performed keeping the same level of complexity (single explicit snow layer). This constraint allowed a simple integration with the ECMWF Integrated Forecast System (IFS) in its several applications ranging from data assimilation for short-range weather forecast to seasonal prediction. Offline validation covering several spatial and temporal scales considered (i) site simulations for several observation locations from SnowMIP2 (section 3), and (ii) global simulations driven by the meteorological forcing from the Global Soil Wetness Project 2 (GSWP2) (Dirmeyer et al. 1999, 2002; Gao et al. 2004) and by ECMWF Re-Analysis (ERA)-Interim (ERA-Interim; Simmons et al. 2007). GSWP2 Results are compared against basin-scale runoff and terrestrial water storage variation (TWSV) in section 4. In section 5 ERA-Interim simulated snow cover fraction and surface albedo are compared with remote sensed products. Model results are presented and discussed throughout the text and the main conclusions of the work are summarized in section 6.

2. Models

a. HTESSEL

HTESSEL represents vertical transfers of water and energy using four vertical layers to represent soil temperature and moisture. The model evaluates the land surface response to the atmospheric forcing and estimates the surface water and energy fluxes along with the temporal evolution of the snowpack, soil temperature, and moisture. At the interface between the surface and the atmosphere, each grid box is divided into fractions (tiles), with up to six fractions over land (bare ground, low and high vegetation, intercepted water, shaded and exposed snow). Each fraction has its own properties defining separate heat and water fluxes used in the energy-balance equation solved for the tile skin temperature. The snow scheme in HTESSEL is an energy- and mass-balance model that represents an additional layer on top of the upper soil layer, with independent prognostic thermal and mass contents. The formulation of the snow mass [or snow water equivalent (SWE)] and energy budgets in HTESSEL are described in the appendix along with the snow density and albedo parameterizations.

b. Revised snow scheme

1) SNOW LIQUID WATER CONTENT

The HTESSEL snow scheme does not account for snow liquid water (SLW) in the snowpack (see appendix). A proper consideration of the SLW requires several modifications: (i) the thermal effects related to the latent heat of fusion (Tribbeck et al. 2006), (ii) changes in the snow runoff [following Rutter et al. (2008), as opposed to the current scheme in which melted snow leaves the snowpack immediately], and (iii) interception of rainfall by the snowpack [as in Bélair et al. (2003) correcting for the rainfall bypass of the snowpack in the current scheme].

The snow energy budget [Eq. (A4)] in the presence of SLW changes can be written as

$$(\rho C)_{\text{sn}} D_{\text{sn}} \frac{\partial T_{\text{sn}}}{\partial t} = R_{\text{sn}}^N - H_{\text{sn}} - L_s E_{\text{sn}} - G_{\text{sn}}^B - L_f M_{\text{sn}} - Q_{\text{sn}}^{\text{INT}}$$

$$Q_{\text{sn}}^{\text{INT}} = L_f M_{\text{sn}}^{\text{INT}} = L_f \frac{\partial S_l}{\partial t}, \quad (1)$$

where $(\rho C)_{\text{sn}}$ is the snow volumetric heat capacity ($\text{J m}^{-3} \text{K}^{-1}$); D_{sn} is the snowpack depth (m); T_{sn} is the snow temperature (K); and the energy fluxes R_{sn}^N , H_{sn} , and G_{sn}^B are the net radiation (shortwave and longwave), sensible heat flux, and basal heat flux (W m^{-2}), respectively. The mass fluxes E_{sn} and M_{sn} are the snow sublimation and melting ($\text{kg m}^{-2} \text{s}^{-1}$), respectively, that are associated with the latent heat of sublimation L_s and

fusion L_f (J kg^{-1}). The superscript INT denotes internal phase changes, where $Q_{\text{sn}}^{\text{INT}}$ is the heat change associated with internal phase changes, and S_l is the snow liquid water content (SLW) (kg m^{-2}). Without loss of generality, it can be assumed that for the grid squares characteristic of NWP,

$$S_l = S_l(T_{\text{sn}}, S, \rho_{\text{sn}}) \approx f(T_{\text{sn}}) S_l^c(S, \rho_{\text{sn}}), \quad (2)$$

where S_l^c (kg m^{-2}) is the snow liquid water capacity, S (kg m^{-2}) is the sum of snow and water in the snowpack (also referred as SWE along the text), and ρ_{sn} is the snow density (kg m^{-3}). The snow temperature function is prescribed in an analytical form—following a similar approach described by Viterbo et al. (1999) for soil phase changes:

$$f(T_{\text{sn}}) = \begin{cases} 0, & T_{\text{sn}} < T_f - d/2 \\ 1 + \sin\left[\frac{\pi(T_{\text{sn}} - T_f)}{d}\right], & T_{\text{sn}} \geq T_f - d/2 \end{cases}, \quad (3)$$

where T_f is the triple-point temperature for water (273.16 K) and d is a characteristic temperature difference, with respect to T_f , limiting the phase change regime. In the numerical implementation $d = 4$ K was chosen. Snow liquid water capacity is approximated as a function of SWE and snow density, following Anderson (1976)

$$S_l^c = S[r_{l,\min} + (r_{l,\max} - r_{l,\min}) \max(0, \rho_{\text{sn},l} - \rho_{\text{sn}})/\rho_{\text{sn},l}], \quad (4)$$

with the constants $r_{l,\min} = 0.03$, $r_{l,\max} = 0.1$ and $\rho_{\text{sn},l} = 200 \text{ kg m}^{-3}$. This equation is a simple parameterization of a very complex phenomenon and has been used recently in other snow schemes for NWP, for example, Boone and Etchevers (2001).

Combining Eqs. (1) and (2) results in a modified snow energy budget equation,

$$\left[(\rho C)_{\text{sn}} D_{\text{sn}} + L_f S_l^c \frac{\partial f(T_{\text{sn}})}{\partial T_{\text{sn}}} \right] \frac{\partial T_{\text{sn}}}{\partial t} = R_{\text{sn}}^N - L_s E_{\text{sn}} - H_{\text{sn}} - G_{\text{sn}}^B - L_f M_{\text{sn}}, \quad (5)$$

with one extra term in the lhs of the equation, that can be interpreted as an additional snow heat capacity—or heat capacity barrier. In compacted snowpacks, the representation of SLW as a diagnostic increases the snow heat capacity by a factor of 5 (Fig. 1). This increase acts as a heat barrier near T_f , representing the increased snow temperature inertia due to freeze–melt events.

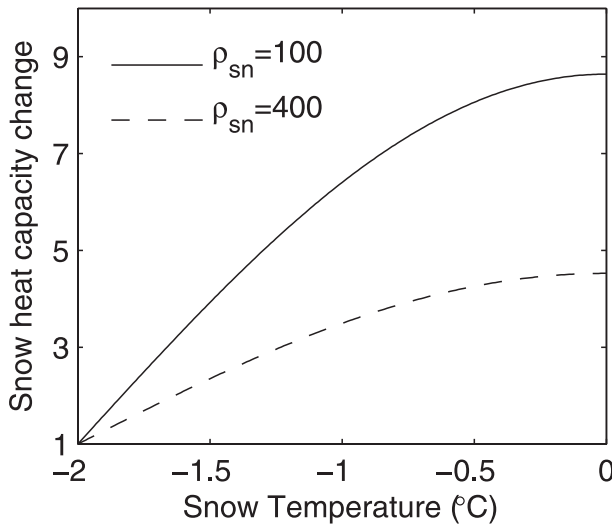


FIG. 1. Ratio between the apparent snow heat capacity [multiplicative term in the lhs of Eq. (5)] and snow heat capacity [multiplicative term in the lhs of Eq. (A4)], as function of snow temperature for constant SWE of 100 kg m^{-2} and snow densities of 100 (solid line) and 400 (dashed line) kg m^{-3} .

This diagnostic approach for SLW also allows the representation of rainfall interception. The new snow mass balance reads as

$$\frac{\partial S}{\partial t} = F + c_{\text{sn}} F_l - c_{\text{sn}} E_{\text{sn}} - R_{\text{sn}}, \quad (6)$$

where F , F_l , and R_{sn} are the mass fluxes of snowfall, rainfall, and runoff ($\text{kg m}^{-2} \text{ s}^{-1}$), and c_{sn} is the snow cover fraction. Rainfall is considered to reach the snowpack at T_f , and the latent heat released by the freezing of the intercepted rainfall, if $T_{\text{sn}} < T_f$, is also accounted in the energy-balance solution. Runoff is defined as the rate at which liquid water leaves the snowpack. Liquid water is generated by melting (M_{sn}) and by rainfall interception (F_l). When snow liquid water content exceeds the snow liquid water capacity [defined in Eq. (4)] runoff is generated.

2) SNOW DENSITY

The original snow density parameterization assumed an exponential evolution toward a maximum density [Eq. (A6)]. In the new scheme, the rate of density change is parameterized as

$$\frac{1}{\rho_{\text{sn}}} \frac{\partial \rho_{\text{sn}}}{\partial t} = \frac{\sigma_{\text{sn}}}{\eta_{\text{sn}}(T_{\text{sn}}, \rho_{\text{sn}})} + \xi_{\text{sn}}(T_{\text{sn}}, \rho_{\text{sn}}) + \frac{\max(0, Q_{\text{sn}}^{\text{INT}})}{L_f(S - S_l)}, \quad (7)$$

where the first two terms represent overburden and thermal metamorphism (Anderson 1976; Boone and

Etchevers 2001), respectively, and the last term represents the compaction related to meltwater retained in the snowpack, adapted from Lynch-Stieglitz (1994). In the overburden term [first term on the rhs of Eq. (7)], σ_{sn} and η_{sn} are the pressure of the overlaying snow (Pa) and snow viscosity (Pa s), respectively. Melted water retained in the snowpack leads to a decrease of snow depth while keeping the SWE constant. Following the original scheme, in snowfall conditions a weighted average is taken between the current snow density and the density of snowfall [see Eq. (A5)]; the updated snow density is used in the rhs of Eq. (7). Snowfall density is changed from a constant value, in the original scheme, to an expression from CROCUS (Brun et al. 1989, 1992) where fresh snow density is a function of near-surface air temperature and wind speed (see also Boone and Etchevers 2001). Snow density is constrained to be between 50 and 450 kg m^{-3} .

3) SNOW COVER FRACTION

Snow cover fraction in the original scheme was only a function of SWE [see Eq. (A2)], whereas the new formulation depends on both SWE and snow density:

$$c_{\text{sn}} = \min\left(1, \frac{S/\rho_{\text{sn}}}{0.1}\right). \quad (8)$$

This new formulation, although very simple, is expected to represent the hysteresis of snow cover between the beginning of the cold season (low snow densities) and the later stage of ablation (high snow densities). In the beginning of the cold season a reduced amount of SWE is needed to fully cover an entire grid box. During the ablation period, the emergence of snow-free patches reflects the need of much more SWE to have a fully covered grid box. Figure 2 shows the different paths of snow cover fraction as function of SWE for a low- and high-density snowpack. The original scheme [Eq. (A2)] lies between the two extremes of snow densities.

4) SNOW ALBEDO

Snow albedo in exposed areas evolves according to the original scheme with an exponential or linear decay in melting and nonmelting conditions, respectively [see Eq. (A7)]. In the revised scheme the melting formulation for albedo decay is also activated when $T_{\text{sn}} \geq T_f - 2$. The representation of SWL as a diagnostic [Eqs. (1)–(3)] is also activated, with internal phase changes, above this temperature threshold. The definition of this temperature threshold for both SLW and albedo decay also accounts for the subgrid-scale variability of the snowpack properties for typical climate and NWP resolutions.

The original snow albedo in exposed areas was reset to its maximum value when $F > 1 \text{ kg m}^{-2} \text{ h}^{-1}$. This

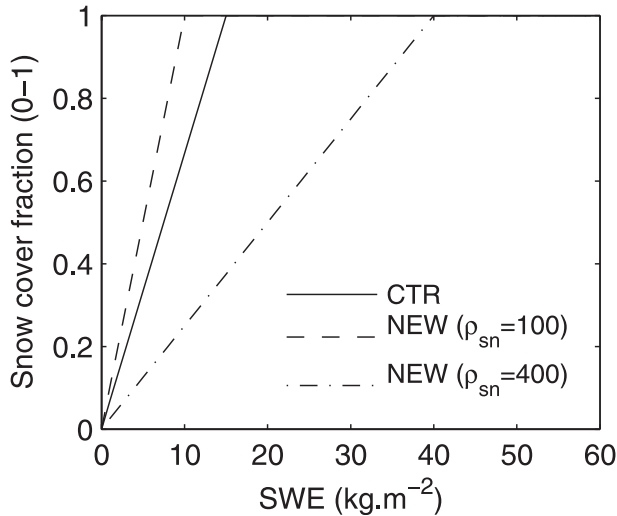


FIG. 2. Snow cover fraction as function of SWE as in the original HTESSEL snow scheme [solid line, Eq. (A2)], and new [Eq. (8)] for snow densities of 100 (dashed line) and 400 (dashed dotted line) kg m^{-3} .

threshold, and its definition, has been reported as a drawback in this type of snow albedo parameterization (Pedersen and Winther 2005; Molders et al. 2008), which is also used in other NWP models. To reduce the importance of the threshold a continuous reset was implemented:

$$\alpha_{\text{sn}}^{t+1} = \alpha_{\text{sn}}^t + \min\left(1, \frac{F\Delta t}{10}\right)(\alpha_{\text{max}} - \alpha_{\text{sn}}^t), \quad (9)$$

where α_{sn} is the snow albedo. Superscripts t and $t + 1$ represent the current and next time step, respectively, and Δt is the model time step (s). This formulation assumes that 10 kg m^{-2} of fresh snowfall are needed to reset the snow albedo to its maximum value ($\alpha_{\text{max}} = 0.85$).

The albedo of shaded snow (snow under high vegetation) was changed from a constant value of 0.15 to a vegetation-type-dependent albedo (Table 1) adapted from Moody et al. (2007). Moody et al. (2007) provide a 5-yr (2000–04) climatological statistics of Northern Hemisphere broadband ($0.3\text{--}5.0 \mu\text{m}$) white-sky albedo for the 16 International Geosphere-Biosphere Program (IGBP) ecosystem classes when accompanied by the presence of snow on the ground. The statistics were obtained using validated, high quality Moderate Resolution Imaging Spectroradiometer (MODIS) land surface albedo data, flagged as snow in the associated quality assurance fields. The retuned forest albedo toward significantly higher values accounts implicitly for trees' intercepted snow effect, which is neglected in the current scheme.

TABLE 1. Mean values of Northern Hemisphere 5-yr (2000–04) broadband surface albedo (in presence of snow) aggregated by high vegetation type (adapted from Moody et al. 2007).

Vegetation type	Albedo
Evergreen needleleaf trees	0.27
Deciduous needleleaf trees	0.33
Deciduous broadleaf trees	0.31
Evergreen broadleaf trees	0.38
Mixed forest–woodland	0.29
Interrupted forest	0.29

3. Site validation

a. Simulation setup and observations

Different sets of experiments were performed (Table 2). These experiments include the original (CTR) and new (NEW) snow schemes and intermediate model configurations with progressive activation of the described changes to the model. All the activated parameterizations were described in the previous section except liquid water prognostic plus rainfall interception (LWPR) and new snow scheme with prognostic liquid water (NEW_PR; Table 2). In those two experiments SLW is represented using a prognostic approach. In this approach a new prognostic equation for SLW was implemented following very simple assumptions: i) SLW only coexists with ice when $T_{\text{sn}} = T_f$; ii) melted snow goes to the SLW reservoir with maximum capacity defined by Eq. (4), and iii) snow runoff is generated when the amount of SLW exceeds the liquid water holding capacity. This parameterization is not described in detail since its formulation is not essential to the discussion.

HTESSEL, with its original snow scheme, participated in the SnowMIP2 intercomparison project. Rutter et al. (2009) and Essery et al. (2009) report the main conclusions of the project along with information regarding the different observational sites, which included five locations with data in both open and forest sites for two winter seasons: Alptal ($47^{\circ}3'N$, $8^{\circ}43'E$, 1200 m, Switzerland), Berms ($53^{\circ}55'N$, $104^{\circ}42'W$, 579 m, Canada), Fraser ($39^{\circ}53'N$, $105^{\circ}53'W$, 2820 m, United States), Hitsujigaoka ($42^{\circ}59'N$, $141^{\circ}23'E$, 2820 m, Japan, only one winter), and Hyytiälä ($61^{\circ}51'N$, $24^{\circ}17'E$, 181 m, Finland) (see also Fig. 8). Near-surface atmospheric forcing data were available for all locations and observations include snow depth, snow density, and SWE. Simulations were performed for all five SnowMIP2 locations summing a total of 18 different cold seasons \times sites. Initial conditions and climatological data were made available by the data providers.

The results of TESSEL presented in Essery et al. (2009) are not identical to the CTR results presented in this paper. The model has the same snow and soil

TABLE 2. Sensitivity experiments acronyms and respective activated parameterizations.

Expt name	Parameterizations activated
CTR	–(see appendix for description)
DENS	Snow density [Eq. (7)]
LWD	Snow density + liquid water diagnostic [Eq. (5) + Eq. (6) setting $F_{l,sn} = 0$]
LWDR	LWD + rainfall interception [Eq. (6)]
LWDR_A	LWDR + exposed snow albedo [Eq. (9)]
LWDR_FA	LWDR + forest snow albedo (Table 1)
LWDR_AFA	LWDR + exposed snow albedo [Eq. (9)] + forest snow albedo (Table 1)
LWDR_SC	LWDR + snow cover fraction [Eq. (8)]
NEW	LWDR_AFA + snow cover fraction [Eq. (8)]
LWPR*	Snow density + liquid water prognostic + rainfall interception
NEW_PR*	LWPR + exposed snow albedo + forest snow albedo + snow cover fraction

* Prognostic representation of snow liquid water content.

hydrology, but the surface roughness lengths were changed from input fields to land cover type dependent. In the present paper, all the simulations were performed with the revised roughness lengths. That modification improved the simulations over forested areas. Such changes are prior to the development of the new snow scheme and, because of its different physical and technical nature, they are not described or discussed here.

b. Snow depth, density, and SWE

Model results and observations of SWE, snow depth, and snow density for the 2004/05 winter season in the Fraser open and forest sites are shown in Fig. 3. CTR and NEW underestimate SWE (Figs. 3a,d) from the beginning of the winter season throughout midspring in both forest and open sites, suggesting either too much melting or excessive sublimation. During the ablation period, CTR showed an early melting in the forest site and a late melting in the open site. These distinct errors between open and forest sites during the ablation period were also observed in other SnowMIP2 locations (not shown). Averaged for all 18 CTR simulations, the final ablation is delayed by 10 days and accelerated by 21 days in open and forest sites, respectively. The NEW snow scheme prediction of final ablation is closer to observations with an average delay of 2 days in open sites (6 out of 9 improved) and an acceleration of 13 days in forest sites (8 out of 9 improved).

Figures 3c,f compare simulated versus observed snow density. Snow density is overestimated by CTR throughout the winter season until the final ablation period when it is underestimated. The simulations show a fast [exponential—Eq. (A6)] density increase in the beginning of the winter, keeping snow density close to its maximum value of 300 kg m^{-3} during the remaining cold season. This behavior was observed in all available locations. The NEW snow density is closer to the observations representing the low densities during the accumulation

stage and the fast increase in the final ablation. Snow depth in CTR and NEW was underestimated in both sites (Figs. 3b,e), resulting from the SWE underestimation. However, NEW snow depth has a reduced error, when compared with CTR, because of the significant improvement of snow density.

c. Snow and soil temperature

Simulated snow and soil temperatures at the Fraser open site during the 2004/05 winter are compared against observations in Fig. 4. Observations of snow temperature were conducted using a thermocouple string at fixed depths, every 10 cm up to 180 cm. Mean snowpack temperature was derived by averaging the thermocouple observations covered by snow, where snow depth was measured using an acoustic sensor. The observed mean snowpack temperature (Fig. 4a) has a lower thermal amplitude than CTR and NEW, and both simulations underestimate snow temperature throughout the cold season. In a single layer snow scheme it is not possible to represent properly the thermal insulation within the snowpack. This explains the differences between simulated and observed mean snowpack temperature. However, at the end of the cold season, NEW reaches the freezing point faster than CTR and stays in an isothermal state, as the observations suggest, while CTR shows some cooling cycles.

Simulated soil temperatures respond to the different basal heat fluxes, due to the increased insulation in NEW, with a faster cooling in CTR when compared with NEW (Figs. 4b,c). This behavior is observed both near the surface and at 50-cm depth. Averaged from December to mid-May CTR has a negative bias of -5.2 and -3.9 K at 5- and 50-cm depth, respectively. NEW reduces significantly the soil temperature bias to -1.8 and -1.3 K at 5- and 50-cm depth, respectively. NEW improves the prediction of final ablation (see Fig. 3d), which affects soil heating after snow disappearance.

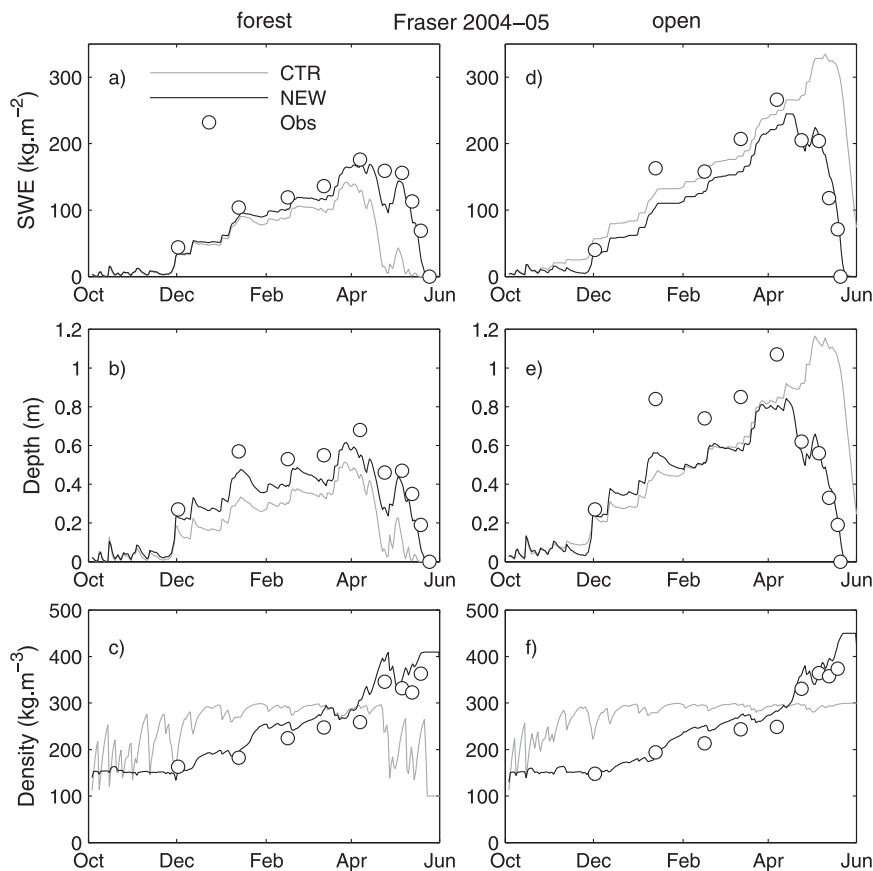


FIG. 3. Simulations results for CTR (gray) and NEW (black) for the 2004/05 winter season at (left) Fraser forest and (right) open sites: (a),(d) SWE, (b),(e) snow depth, and (c),(f) snow density. Observations are represented by open circles.

There is a reduction of the soil temperature bias near the surface by the end of May from -11.4 K in CTR to -2.8 K in NEW.

d. Sensitivity to activated parameterizations

Sensitivity tests, where the components of NEW were gradually activated, are detailed in Table 2. The comparison was made to the root-mean-square errors (RMSE) in modeled SWE normalized by standard deviations of the observations (errors in snow depth, rather than SWE, were calculated for Hitsujigaoka and Hyytiälä open sites). Figure 5 summarizes the RMSE for all locations classified as open or forest sites. The new snow density (DENS) has a limited impact on SWE simulation, whereas, when combined with SLW representation [liquid water diagnostic (LWD)], it improves SWE in forest sites. The interception of rainfall in the snowpack (LWDR) has also a positive impact on forest sites simulations, while keeping the open plots unchanged. The changed albedo formulation (LWDR_AFA) shows a significant improvement in open sites, with a small impact on forest sites. When all the

new components are activated (NEW) the RMSE of SWE is lower than any of the other experiments in both open and forest sites. Open sites had a delayed ablation in CTR, which was mainly reduced with the new exposed albedo formulation. The early ablation in forest sites was corrected mainly by the incorporation of SLW. This shows that the underlying physical processes responsible for the observed biases in open and forest sites were of different nature: i) early melting in forest sites due to neglecting the refreezing of melted liquid water and ii) late melting in open sites due to an underestimation of absorbed solar radiation resulting from an overestimation of snow albedo.

SLW is often represented in snow schemes following a prognostic approach. The experiments LWPR and NEW_PR were conducted to analyze the impact of such approach when compared to the diagnostic implementation described in this paper. This simple validation aims to examine whether the approaches are comparable, not to decide which one is better. The RMSE of SWE in LWPR is comparable with LWDR for forest sites, but

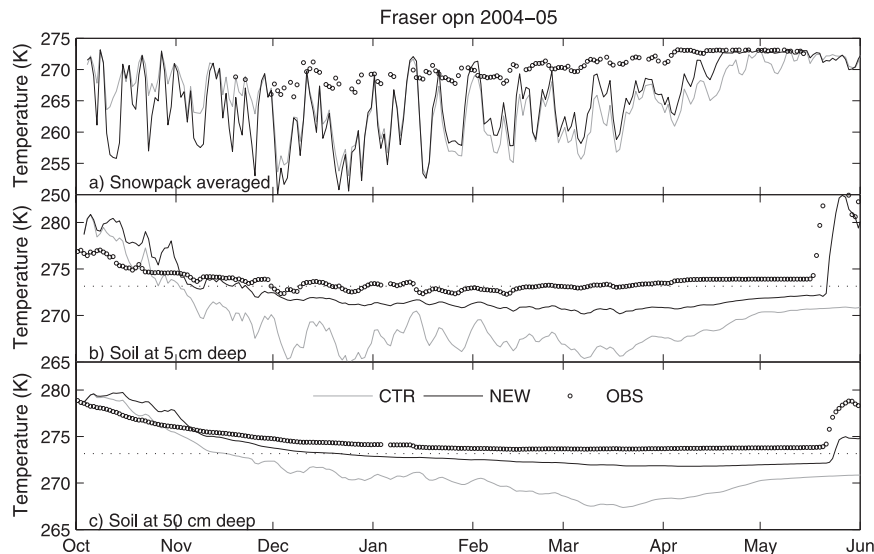


FIG. 4. Model-simulated (a) snow temperature and soil layer temperature at (b) 5-cm depth and (c) 50-cm depth by CTR (gray) and NEW (black) for the 2004/05 winter season in Fraser open site. The simulations and observations (open circles) represent daily means.

LWPR has a better performance than LWDR in open plots. On the other hand, the inclusion of all physical mechanisms in NEW_PR dilutes the advantages of the prognostic water reservoir.

4. Basin-scale validation

a. Simulation setup

GSWP2 provides a set of near-surface forcing to drive land surface schemes in an offline mode. The atmospheric forcing data are provided at a resolution of 1° globally. In the current work, we have used the latest release of GSWP2 atmospheric forcing based on the 40-yr ECMWF Re-Analysis (ERA-40; Uppala et al. 2005) where only precipitation is corrected using the Global Precipitation Climatology Project (GPCP) dataset. The dataset is available for the period January 1986 to December 1995. Surface pressure, air temperature, and specific humidity at 2 m, and wind at 10 m, are provided as instantaneous values. Downward surface radiation fluxes and precipitation fluxes represent 3-h averages. Climatological data, such as land-cover and vegetation types, were interpolated to a $1^\circ \times 1^\circ$ grid from ERA-40.

b. Basins and observations

Terrestrial water storage is the sum of all forms of water storage on the land surface. Seasonal and interannual variations in storage are determined by the combined effect of soil moisture, groundwater, snow cover, and surface water. Diagnostics of monthly TWSV for 41

midlatitude basins all over the globe were used to validate the new snow scheme. The Basin Scale Water Balance (BSWB) dataset described in Hirschi et al. (2006) was derived with the combined atmospheric and terrestrial water-balance approach (Seneviratne et al. 2004) using conventional streamflow measurements and vertically integrated atmospheric moisture convergence data from ERA-40. The runoff data are partially composed of data from the Global Runoff Data Centre (GRDC) and other local sources. In the following discussion HTESSEL simulations were spatially aggregated for each basin.

Such large-scale basins are composed by many types of land cover, rivers, and lakes, each one with different hydrological characteristics. Simulated integrated values such as runoff and TWSV were spatially averaged. This simple procedure neglects river routing and effects of water and soil freezing. Such processes may delay basin streamflow when compared with instantaneous local runoff. However, the BSWB dataset consists of monthly data, which are compared against time-averaged monthly simulated fluxes. This approach has been also used by Balsamo et al. (2009) during the validation of HTESSEL soil hydrology.

c. Impact in the Ob basin

The Ob River is a major river in western Siberia, Russia. The basin consists mostly of steppe, taiga, swamps, tundra, and semidesert, with an average high vegetation fraction of 50%. Basin-averaged simulated SWE, snow density, percentage of frozen surface, and runoff are presented in Fig. 6 for the 1989–90 period. SWE simulated by

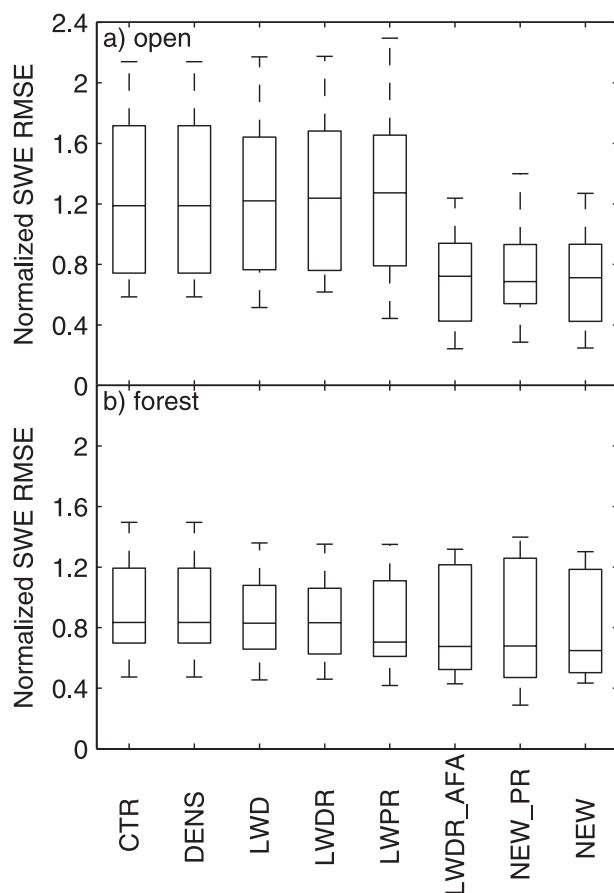


FIG. 5. Box plot summaries describing the normalized RMSE of SWE for different model configurations, combined at all SnowMIP2 locations at (a) open sites and (b) forest sites. The boxes have horizontal lines at the lower quartile, median, and upper quartile and the whiskers (vertical lines) extend from the end of each box to $1.5 \times$ the interquartile range; outliers beyond this range are represented by + symbols.

the new snow scheme is higher than in CTR (Fig. 6a). The interception of rainfall in the snowpack was 53 mm, while snowfall was 218 mm. The additional accumulation of 53 mm to the snowpack in NEW explains the differences in SWE, resulting in a 14-day difference during final ablation between NEW and CTR. As in the SnowMIP2 Fraser site simulations (Fig. 3), snow density is lower in NEW throughout the winter, reaching higher values than CTR only during the ablation period.

Lower snow density and higher SWE result in a thicker snowpack, with an increased insulation effect. The percentage of frozen soil in Fig. 6c is the fractional basin area where the first soil layer (0–7 cm) is frozen. The increased insulation in NEW reduces soil cooling, which reduces soil freezing. In CTR the basin surface is completely frozen from January to mid-February, while in NEW only 20%–30% of the basin is frozen. The runoff partitioning between surface and bottom

drainage is shifted in NEW, with a reduction of surface runoff (Fig. 6d) and an increase of bottom drainage (Fig. 6e). In HTESSEL all rainfall and melted water are discharged as surface runoff when the first soil layer is frozen. The NEW snow scheme reduces soil freezing, thereby reducing surface runoff and increasing soil water storage. The overall impact in total runoff is represented in Fig. 6f where NEW and CTR are compared against BSWB monthly data. The peak runoff date is accelerated and volume overestimated by CTR and NEW. However, the NEW snow scheme improves both the timing and magnitude of the total basin runoff.

d. Monthly TWSV and runoff

Figure 7 compares the mean annual cycles of simulated runoff and TWSV with BSWB data over the Ob and Mackenzie basins. The mean annual cycles of CTR runoff show an early peak in both basins with overestimation in the Ob but with a correct volume in Mackenzie. Both timing and volume are improved in NEW over the Ob basin (as discussed before), while the volume in the Mackenzie is poorer than in CTR. The simulated TWSV in CTR displays timing errors similar to the runoff in both basins. The increased water storage during spring in NEW resulted in a better agreement with BSWB TWSV during summer. The reduction of total runoff in both basins in NEW was compensated by an increase in evapotranspiration, especially during spring (not shown). Less soil freezing and early thaw increase evapotranspiration in NEW, since more water is available for the plant root uptake.

Table 3 summarizes the RMSE of runoff in 10 high-latitude basins, corresponding to the subset of the original 41 basins of the BSWB dataset where more than 30% of available data has mean snow cover duration exceeding 100 days. The mean snow cover duration was calculated for all grid points and then averaged for each basin using the CTR simulation. For all the basins with snow cover duration less than 100 days the differences between CTR and NEW are negligible. This result is due to the smaller impact of snow in the hydrological cycle.

The last two columns of Table 3 compare the runoff RMSE between the diagnostic (LWDR) and the prognostic (LWPR) formulation to represent SLW. The differences between the two formulations are small. The inclusion of the new snow cover fraction, exposed albedo, and forest albedo (NEW) to LWDR also shows a small effect in the runoff. The similar performance of NEW, LWDR, and LWPR, very distinct from CTR, is an indication that the new snow density is the most important change. As discussed before, the original scheme suffered from a lack of soil water storage due to excessive surface runoff. Averaged over all 10 basins, NEW

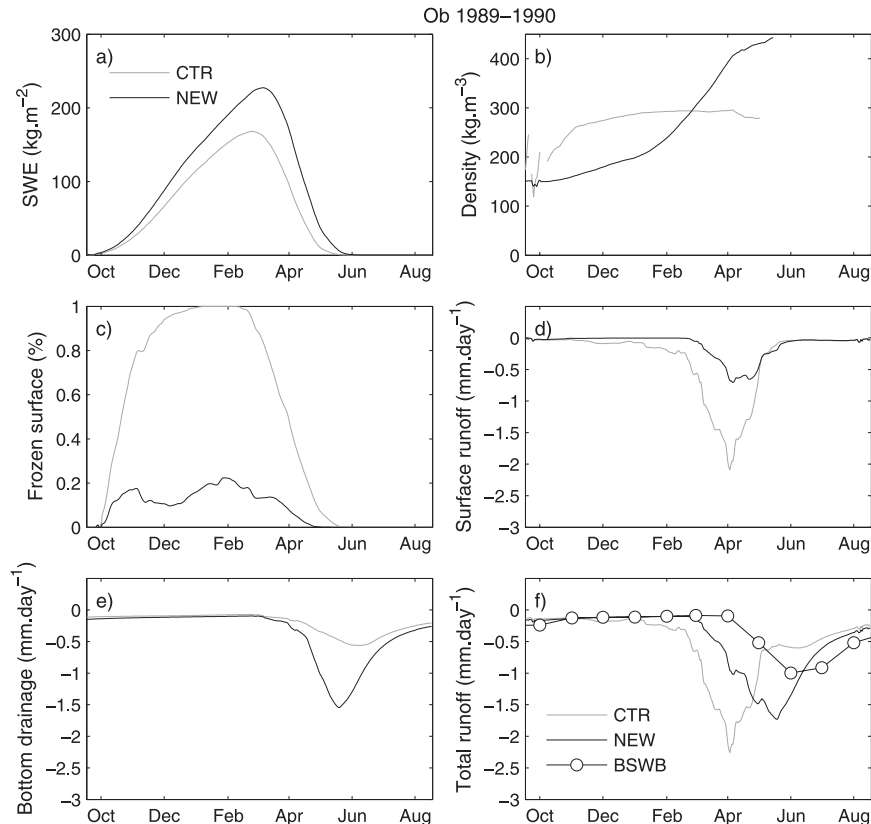


FIG. 6. Simulation results for CTR and NEW during the period October 1989 to August 1990 spatially averaged for the Ob basin: (a) SWE, (b) snow density, (c) fraction of basin area frozen at the surface, (d) surface runoff, (e) bottom drainage, and (f) total runoff. Total runoff simulations are compared with monthly BSWB data. Simulated daily data were smoothed with a 30-day moving average.

reduces the runoff RMSE by 0.24 mm day^{-1} (32% of the CTR). With the exception of the Neva River basin, any of the three new formulations performs better than CTR.

Figure 8 represents the location and runoff RMSE improvement between NEW and CTR for the 10 basins listed in Table 3. The figure highlights central Siberia as the area with higher improvements in runoff. These results show that the inclusion of the new snow density, with higher insulation, was more effective in flat terrain areas dominated by low vegetation/bare ground, where the shading effects of high vegetation and subgrid orography variability (not addressed in this model revision, and with a very simplified treatment in the model) play a secondary role.

5. Global validation

a. Simulation setup

ERA-Interim reanalysis covers the period January 1989 to the present. The atmospheric forcing data were gridded on the original Gaussian reduced grid N128 (resolution of 0.7° over the equator) globally at 3-h intervals. The

state variables are provided as instantaneous values from the lowest model level (approximately 10 m above the surface) and correspond to the 3–12-h forecast interval from initial conditions at 0000 and 1200 UTC. Surface precipitation and radiation fluxes represent 3-h averages. To avoid the initial spinup in precipitation, the 3-hourly surface fluxes are taken from the 9–21-h forecasts initialized at 0000 and 1200 UTC.

Unlike GSWP2, ERA-Interim precipitation was not corrected with GPCP (or other) observational dataset. Errors in total precipitation and partitioning between liquid and solid rainfall may produce biases in the simulated snowpack. Such corrections are out of the scope of the present work. Nevertheless, the ERA-Interim dataset has already been explored in offline LSM works (Balsamo et al. 2010; Dutra et al. 2010).

b. Snow cover

1) IMS NOAA/NESDIS SNOW COVER

The interactive Multisensor Snow and Ice Mapping System (IMS) is a workstation-based application, which

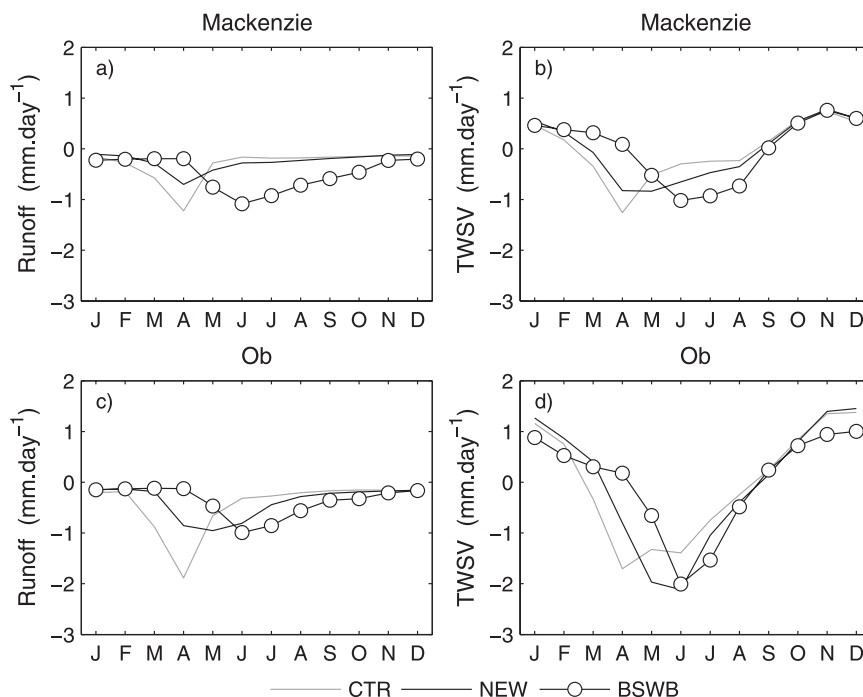


FIG. 7. Mean annual cycles of (a),(c) runoff and (b),(d) TWSV in (top) Mackenzie and (bottom) Ob basins simulated by CTR and NEW during GSWP-2 period and compared with BSWB data.

allows the analyst to process various snow cover data in a manner timely enough to release a real-time daily product (Helfrich et al. 2007; Ramsay 1998). Northern Hemisphere (NH) snow-covered maps are primarily based on satellite imagery. In addition, the analyst can rely on station data and the previous day's analysis. Since February 1997, the IMS product has been produced daily at approximately 24-km resolution (1024×1024 grid).

This dataset has already been applied to the validation of model-simulated snow cover extent in other studies (e.g., Sheffield et al. 2003). IMS National Oceanic and Atmospheric Administration/National Environmental Satellite, Data, and Information Service (NOAA/NESDIS) snow cover product (NOAA/NESDIS/OSDPD/SSD 2006) was spatially aggregated to the N128 Gaussian reduced grid. Fractional snow cover in the Gaussian grid

TABLE 3. RMSE of simulated vs BSWB runoff in 10 high-latitude basins. Simulations forced by GSWP2 for the period 1986–95. For each basin are presented the catchment area (adapted from Hirschi et al. 2006), mean snow cover (SC) duration, and mean annual amplitude of runoff.

Basin	Catchment area (km ²)	SC duration (days)	Runoff (mm day ⁻¹)	Runoff RMSE (mm day ⁻¹)			
				CTR	NEW	LWDR	LWPR
1) Yukon	779 081	198	2.18	0.95	0.53	0.58	0.58
2) Podka ^a	209 591	190	3.47	0.90	0.45	0.50	0.57
3) Lena	2 351 052	182	3.07	0.96	0.84	0.86	0.87
4) Tom	62 830	158	6.92	1.88	1.59	1.68	1.64
5) Ob	2 859 889	154	1.06	0.69	0.32	0.34	0.38
6) Yenisei	2 513 361	151	2.79	0.77	0.46	0.51	0.54
7) Mackenzie	1 587 878	140	1.34	0.55	0.42	0.45	0.44
8) Volga	1 333 747	137	1.16	0.65	0.53	0.55	0.57
9) Irtish	403 309	129	0.41	0.42	0.22	0.21	0.25
10) Neva	233 423	116	0.80	0.60	0.63	0.64	0.63
Average ^b	12 334 161 ^c	157	1.96	0.75	0.51	0.54	0.56

^a Podkamennaya Tunguska.

^b Average weighted by catchment area.

^c Total catchments area.

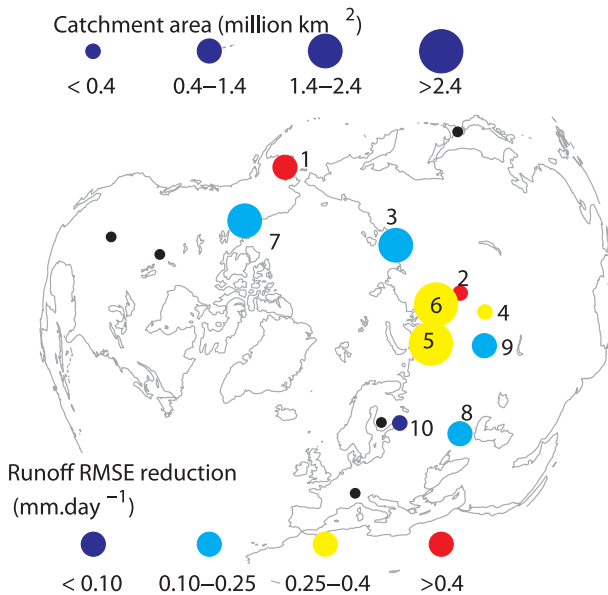


FIG. 8. Basin locations represented by colored symbols. Each basin is numbered as in Table 3 and the location refers to the runoff station observations from Hirschi et al. (2006). The catchment area is associated to the size of the symbol, and the runoff RMSE difference between NEW – CTR is represented by the symbol face color. The black symbols represent the five SnowMIP2 sites.

was evaluated from the original “snow-free/100% snow-covered” binary information. Snow cover fraction was calculated by counting all the 100% snow-covered pixels of NOAA/NESDIS lying within each N128 grid box.

2) SNOW COVER SIMULATIONS

NH simulated snow-covered area is compared against NOAA/NESDIS in Fig. 9. Snow-covered area maximum extents exceed 40 million km², which is coherent with the results presented by Brown and Armstrong (2008). The differences between simulated and NOAA/NESDIS (Fig. 9b) show a distinct annual cycle. The bias is reduced during low variability periods, namely summer and late winter. On the other hand, the bias increases during the high variability accumulation and ablation seasons. During the initial accumulation period both CTR and NEW show a growing underestimation of snow-covered area that reaches roughly 6 million km². After the initial accumulation, NEW reduces the bias significantly near the peak snow-covered area. During spring, both schemes tend to ablate snow cover too quickly, with increasing underestimation. This behavior was also documented by Frei et al. (2005) in the AGCMs participating in phase 2 of the Atmospheric Model Intercomparison Project (AMIP-2). Averaged over the entire period (January 1999 to December 2008) CTR and NEW have a negative bias in snow-covered area of

3.1 and 1.6 million km², respectively. During spring, CTR and NEW biases are higher: 5.3 and 2.6 million km². LWDR_SC (all new components of NEW except the exposed and forest albedo) simulation partially reduces the bias of CTR with a negative bias in snow-covered area of 2.5 and 4.4 million km², during the whole period and spring, respectively, showing that the new snow cover fraction [Eq. (8)] has an important effect in the model-simulated snow cover extent. The simulated snow-covered area RMSE normalized by the observations temporal standard deviation are 25%, 21%, and 15% for CTR, NEW, and LWDR_SC, respectively.

The NOAA/NESDIS data compose a daily product allowing for a more detailed comparison with simulations. Figure 10 presents the spatial distribution of the frequency of missing snow cover in the simulations during spring, defined as the frequency of occurrence of snow-covered NOAA/NESDIS ($c_{sn} > 0.75$) and simulated snow free ($c_{sn} < 0.25$). Drusch et al. (2004) applied a similar diagnostic to validate the snow depth analysis system in ECMWF. Scandinavia, western Russia, and central/eastern Canada are dominated by high-frequency snow cover missing in CTR (Fig. 10a), reaching one month (30%) in some localized areas. These results agree with the pronounced underestimation of snow-covered area during spring in CTR, analyzed before. NEW reduces the missing snow cover during spring, when compared with CTR, up to a factor of 2 in areas where CTR has higher errors.

c. Surface albedo

1) MODIS ALBEDO

The MODIS albedo product MCD43C3 provides data describing both directional hemispheric reflectance (black-sky albedo) and bihemispherical reflectance (white-sky albedo). Both black-sky and white-sky albedos are available in seven different bands and aggregated visible, near infrared and broadband shortwave. Both *Terra* and *Aqua* platforms are used in the generation of this product. The product also includes snow-free and quality parameters, and is produced every 8 days with 16 days of acquisition projected to a 0.05° grid. These data are distributed by the Land Processes Distributed Active Archive Center (LP DAAC), located at the U.S. Geological Survey (USGS) Earth Resources Observation and Science (EROS) Center (<https://lpdaac.usgs.gov/>). The accuracy and quality of this albedo product have been evaluated by Stroeve et al. (2005), Salomon et al. (2006), Shuai et al. (2008), and Román et al. (2009). The white-sky broadband shortwave albedo was spatially aggregated from the original 0.05° grid to the N128 Gaussian reduced grid.

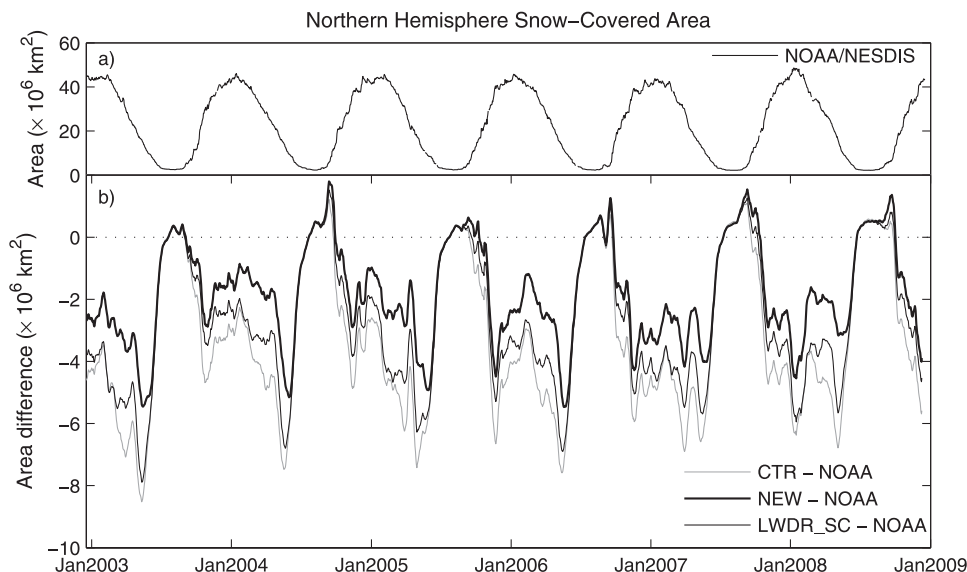


FIG. 9. (a) Northern Hemisphere daily snow-covered area from NESDIS and (b) snow-covered area differences between simulations and NESDIS. Note the different order of magnitude in the vertical axis between the two panels.

2) ALBEDO SIMULATIONS

Figure 11a compares simulated albedo against MODIS-derived albedo in the snow-covered area in the NH. In the following discussion, snow-covered area was derived from the MODIS Percent_Snow layer. Therefore, the mean fractional land area with available data (top of each panel in Fig. 11) excludes snow-free MODIS grid boxes and also

missing data (e.g., because of cloud cover or low quality of the albedo inversion algorithm).

CTR albedo shows a systematic negative bias that increases in magnitude throughout the cold season until May. The exposed albedo parameterization by itself (LWDR_A) improves the simulation in all months except October. The new lookup table for shaded snow (LWDR_FA) has a positive impact in all months. The

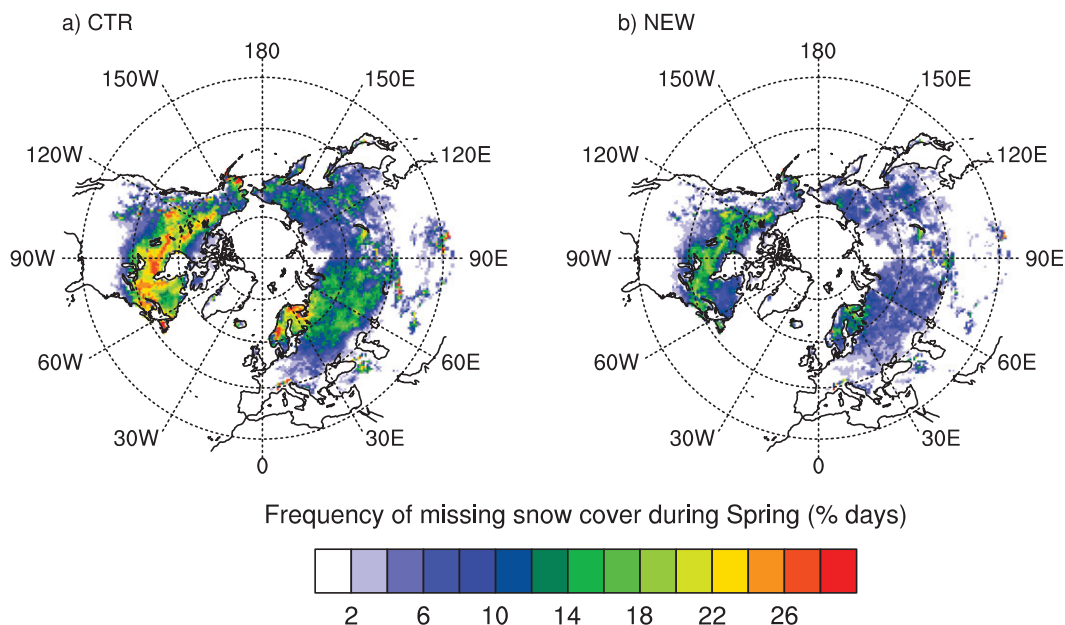


FIG. 10. Frequency of occurrence of snow-covered NESDIS data ($c_{sn} > 0.75$) and simulated snow-free ($c_{sn} < 0.25$) during spring (March–May) for ERAI simulations in the period 2001–08 by (a) CTR and (b) NEW. The number of days in each grid box is normalized by the total number of days of the season.

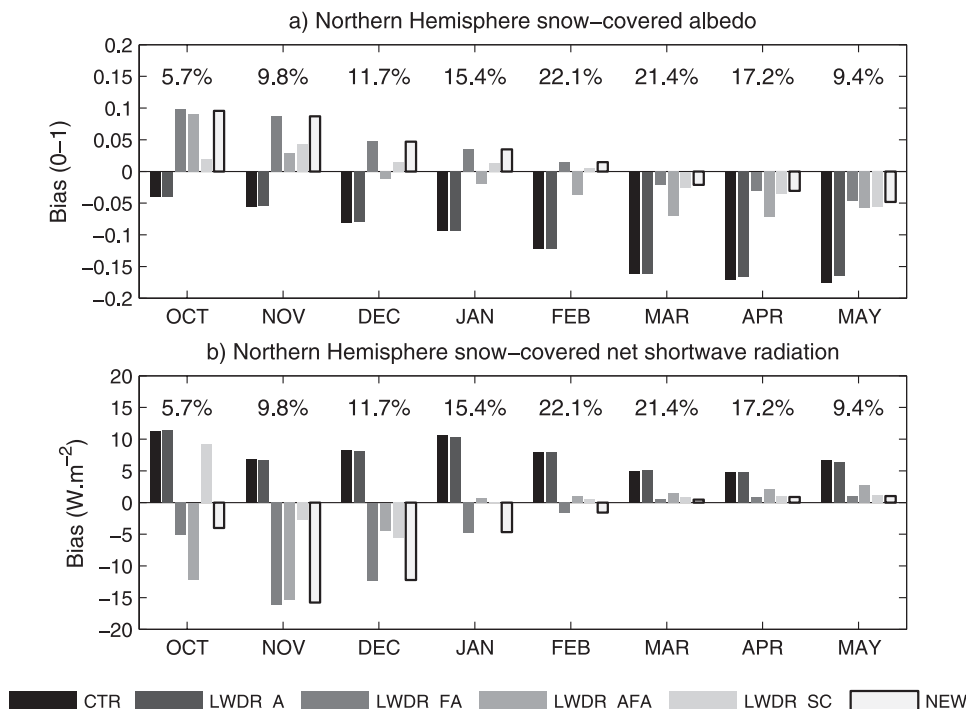


FIG. 11. Monthly bias (simulation – observation) of (a) albedo and (b) net shortwave radiation calculated only over snow-covered grid boxes over the Northern Hemisphere. The fractional snow-covered land of Northern Hemisphere used in the calculations for each month is presented in the top of each graphic. ERAI simulations of albedo and net shortwave radiation are compared against MODIS albedo for the period Jan 2000 to Dec 2008.

NEW snow scheme significantly reduces the albedo bias in all months except October and November. During these two months the signal shift of the albedo bias (from negative in CTR to positive in NEW) and increased magnitude is due to the new exposed albedo parameterization (cf. LWDR_A with LWDR_FA in Fig. 11a). Groisman et al. (1994b) showed that the impact of snow cover in the planetary albedo has the greatest magnitude in spring. Therefore, the degradation of simulated albedo in NEW during late autumn should have a smaller impact than the improvements during late winter and spring. The new snow cover fraction by itself (LWDR_SC) has results similar to CTR, showing that the improved simulated albedo is mainly due to the modified exposed and shaded snow parameterizations.

The impact of albedo biases on the snowpack is modulated by the amount of available solar radiation. Net shortwave radiation (SWnet) is not a direct MODIS product. It was diagnosed using MODIS albedo and ERAI downward shortwave radiation and is compared against simulations in Fig. 11b. The above-mentioned CTR albedo negative bias is reflected in a positive SWnet bias during the entire snow-covered season. On the other hand, NEW SWnet bias is close to zero during

late winter and spring but shows a negative bias in November and December. The reasons for this bias were discussed before. Averaged results from October to May and weighted by the snow-covered area, CTR has a mean positive bias of $+7.1 \text{ W m}^{-2}$, while NEW has a mean negative bias of -1.9 W m^{-2} . In absolute terms, NEW reduces the SWnet bias by 5.2 W m^{-2} when compared with CTR. The area where such flux differences are found covers 14% of the NH land.

Figure 12 represents the mean (2000–08) spring MODIS albedo and respective simulated differences. The differences between simulated and MODIS albedo (Figs. 12b,c) are shown only for snow-covered grid boxes flagged by MODIS with at least 50% of feasible data (excluding areas with systematic missing values in MODIS). The negative bias of CTR albedo (Fig. 12b) during spring spreads widely over the entire Northern Hemisphere. There are three main regions with an accentuated bias: northeast Asia, central Asia (north of the Caspian and Aral Seas), and northern Canada. These areas are dominated by low vegetation (tundra and short grass). NEW partially reduces the albedo bias over low vegetation areas, while over high vegetation areas the bias is close to zero. There are some small positive biases in

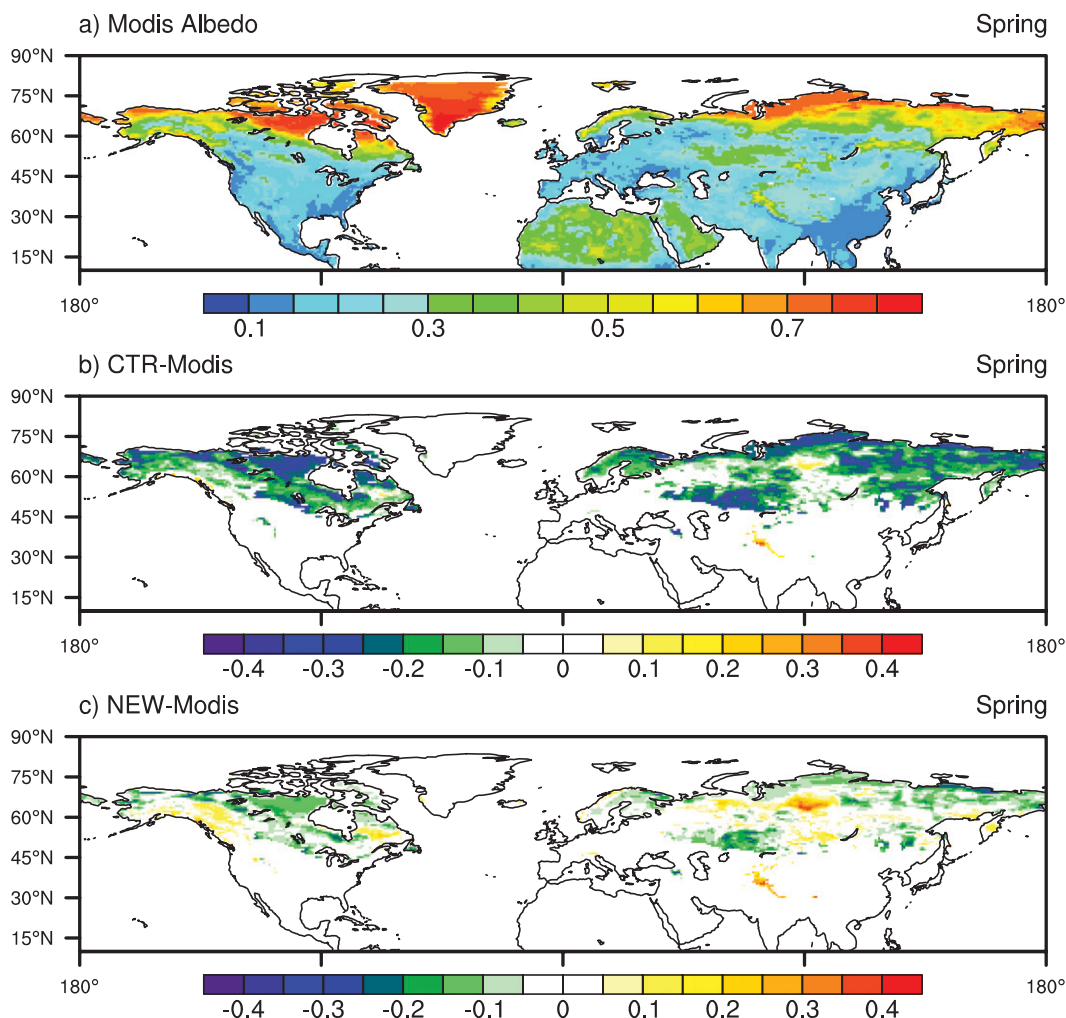


FIG. 12. (a) Mean observed maps of spring albedo by MODIS for the period 2000–08 and differences between simulated albedo and MODIS for (b) CTR and (c) NEW. The differences (b) and (c) show only snow-covered grid boxes with <50% MODIS missing data. Note the different color scales between panel (a) and panels (b) and (c).

NEW on the southern borders of tundra regions (areas dominated by bogs and marshes) in both continents.

6. Conclusions

An improved snow scheme for HTESSEL was presented and validated. The new scheme revises the formulations of snow cover fraction and snow albedo and included a new snow density parameterization and representation of SLW using a diagnostic approach. An offline validation covering several spatial and temporal scales considered (i) site simulations for several observational locations from SnowMIP2 and (ii) global simulations driven by the meteorological forcings from GSWP2 and ERAI.

SnowMIP2 simulations revealed that the original snow scheme had a systematic early and late prediction

of the final ablation in forest and open sites, respectively. The NEW scheme reduces the negative timing bias in forest plots from 21 to 13 days and the positive bias in open plots from 10 to 2 days. The new snow density parameterization in NEW has a good agreement with observations, resulting in an augmented insulation effect of the snowpack. The increased insulation and the new exposed and shaded albedo change the surface energy fluxes. There is a reduction of the basal heat flux that reduces the cooling of the underlying soil, which is warmer in NEW than in CTR during the cold season. Thus, reduced soil freezing decreased the surface runoff and increased soil water storage. The mean annual cycles of runoff and TSWV analyzed for the Ob and Mackenzie basins are closer to the observations in NEW. In 10 Northern Hemisphere basins, there is an average reduction of the monthly runoff RMSE from 0.75 to

0.51 mm day⁻¹ when comparing CTR and NEW, respectively. These results illustrate the importance of snow insulation on the hydrological cycle, even at regional scales.

On a hemispheric scale, the new snow scheme reduces the negative bias of snow-covered area, especially during spring. On a daily scale, using NOAA/NESDIS snow cover data, the early ablation in CTR is reduced by a factor of 2 in some identified regions over the Northern Hemisphere. The changes in snow-covered area are closely related with the changes in surface albedo. The original snow scheme had a systematic negative bias in surface albedo, when compared against MODIS remote sensing data. The new scheme reduced the albedo bias, consequently reducing the spatial- (only over snow-covered areas) and time- (October to November) averaged surface net shortwave radiation bias from +7.1 W m⁻² in CTR to -1.8 W m⁻² in NEW.

For each validation dataset, sensitivity experiments were performed to assess the impact of the new components of the presented snow scheme. Prognostic and diagnostic SLW representations display similar skill in SnowMIP2 (RMSE of SWE) and GSWP2 (RMSE of basin runoff) simulations. Simulated improvements of SWE in SnowMIP2 locations were mainly due to SLW representation on forest sites and due to the new exposed albedo on open sites. The increased snow insulation effect, due to the new snow density parameterization, had an important role on the basins' water balance. Impacts of the new snow cover fraction and exposed and shaded albedo parameterizations were evident when validating against remotely sensed data. Sensitivity tests highlight the role of the different components of the snow scheme with the behavior conditioned by the climate and vegetation conditions of each site. Thus, a robust verification of a LSM model should include a variety of different (and independent) validation datasets.

The present offline methodology is recurrent in validations of LSM (e.g., Boone and Etchevers 2001) and in intercomparison projects (e.g., Rutter et al. 2009). However, the associated nature of the one-way coupling has shortcomings due to the absence of atmospheric response. A complete validation can only be achieved with atmospherically coupled simulations. Tests have been performed and the new snow scheme showed improvements in the simulated near-surface temperature during winter over snow-covered areas; such results will be reported in future work. Future developments of HTESSEL snow scheme will focus on improvements of the representation of snowpack physics (e.g., via the development of a multilayer scheme), and on the coupling with the atmosphere, especially in forested regions. The NEW snow scheme described in this paper

was introduced in the ECMWF operational forecast system in September 2009 (cycle 35R3).

Acknowledgments. The authors thank SnowMIP2 data providers: David Gustafsson and Manfred Stähliand (Alptal—Switzerland); Alan Barr and Paul Bartlett (Berms—Canada); Kazuyoshi Suzuki and Tomoyoshi Hirota (Hitsujioka—Japan); Nuria Altimir and Timo Vesala (Hyytiälä—Finland); and Richard Essery and Nick Rutter for the project organization and useful comments. The BSWB dataset was kindly provided by Martin Hirschi. We also thank the MODIS Land and Albedo teams and in particular Crystal Schaaf for the valuable support and comments regarding the use of MODIS albedo product. The comments of three anonymous reviewers are gratefully acknowledged. This work was supported by the Portuguese Foundation for Science and Technology (FCT) under project AMIC PTDC/AAC-CLI/109030/2008 cofinanced by the European Union under program FEDER. E. Dutra acknowledges the financial support of FCT under Grant SFRH/BD/35789/2007 and Fundação Calouste Gulbenkian.

APPENDIX

HTESSEL Snow Scheme

The snow mass budget reads as

$$\frac{\partial S}{\partial t} = F - c_{\text{sn}} E_{\text{sn}} - M_{\text{sn}}, \quad (\text{A1})$$

where the symbols are defined in the section 2b. The snow fraction is given by

$$c_{\text{sn}} = \min\left(1, \frac{S}{15}\right). \quad (\text{A2})$$

Snow mass and snow depth are related by

$$D_{\text{sn}} = \frac{S}{\rho_{\text{sn}} c_{\text{sn}}}, \quad (\text{A3})$$

where D_{sn} is snow depth (m) in the snow-covered area (D_{sn} is not a grid-averaged quantity).

The snow energy budget reads as

$$(\rho C)_{\text{sn}} D_{\text{sn}} \frac{\partial T_{\text{sn}}}{\partial t} = R_{\text{sn}}^N - L_s E_{\text{sn}} - H_{\text{sn}} - G_{\text{sn}}^B - L_f M_{\text{sn}}. \quad (\text{A4})$$

In this formulation the liquid water fraction is neglected. The snow thermal conductivity changes with changing snow density and is related to the ice thermal conductivity according to Douville et al. (1995).

Following Douville et al. (1995) snow density is assumed to be constant with depth and to evolve exponentially toward a maximum density (Verseghy 1991). First, a weighted average is taken between the current density and the minimum density for fresh snow, giving

$$\rho_{\text{sn}}^* = \frac{S\rho_{\text{sn}}^t + \Delta t F \rho_{\text{min}}}{S + \Delta t F}, \quad (\text{A5})$$

where ρ^* is an intermediate snow density, and after an exponential relaxation is applied,

$$\rho_{\text{sn}}^{t+1} = (\rho_{\text{sn}}^* - \rho_{\text{sn}_{\text{max}}}) \exp(-\tau_f \Delta t / \tau_1) + \rho_{\text{sn}_{\text{max}}}, \quad (\text{A6})$$

where $\tau_1 = 86400$ s, and $\tau_f = 0.24$ are time scales, with minimum density $\rho_{\text{sn}_{\text{min}}} = 100 \text{ kg m}^{-3}$ and maximum density $\rho_{\text{sn}_{\text{max}}} = 300 \text{ kg m}^{-3}$.

Snow albedo in exposed areas evolves according to the formulation of Baker et al. (1991), Verseghy (1991), and Douville et al. (1995) differing for melting and non-melting conditions:

$$\alpha_{\text{sn}}^{t+1} = \begin{cases} \alpha_{\text{sn}}^t - \tau_a \Delta t / \tau_1, & M_{\text{sn}} = 0 \\ (\alpha_{\text{sn}}^t - \alpha_{\text{min}}) \exp(-\tau_f \Delta t / \tau_1) + \alpha_{\text{min}}, & M_{\text{sn}} > 0 \end{cases}, \quad (\text{A7})$$

where $\alpha_{\text{min}} = 0.5$ and $\alpha_{\text{max}} = 0.85$. If snowfall $F > 1 \text{ kg m}^{-2} \text{ h}^{-1}$, the snow albedo is reset to the maximum value $\alpha_{\text{sn}}^{t+1} = \alpha_{\text{max}}$. The albedo for shaded snow is fixed at 0.15. A detailed description of the scheme can be found online at <http://www.ecmwf.int/research/ifsdocs/CY28r1/Physics/index.html>.

REFERENCES

- Anderson, E. A., 1976: A point energy and mass balance model of a snow cover. NOAA Tech. Rep. NWQ 19, 150 pp.
- Armstrong, R. L., and E. Brun, Eds., 2008: *Snow and Climate: Physical Processes, Surface Energy Exchange and Modeling*. Cambridge University Press, 222 pp.
- Baker, D. G., R. H. Skaggs, and D. L. Ruschy, 1991: Snow depth required to mask the underlying surface. *J. Appl. Meteor.*, **30**, 387–392.
- Balsamo, G., P. Viterbo, A. Beljaars, B. Van den Hurk, A. K. Betts, and K. Scipal, 2009: A revised hydrology for the ECMWF model: Verification from field site to terrestrial water storage and impact in the Integrated Forecast System. *J. Hydrometeorol.*, **10**, 623–643.
- , E. Dutra, V. M. Stepanenko, P. Viterbo, P. M. A. Miranda, and D. V. Mironov, 2010: Deriving an effective lake depth from satellite lake surface temperature data: A feasibility study with MODIS data. *Boreal Environ. Res.*, **15**, 178–190.
- Bélair, S., R. Brown, J. Mailhot, B. Bilodeau, and L. P. Crevier, 2003: Operational implementation of the ISBA land surface scheme in the Canadian regional weather forecast model. Part II: Cold season results. *J. Hydrometeorol.*, **4**, 371–386.
- Boone, A., and P. Etchevers, 2001: An intercomparison of three snow schemes of varying complexity coupled to the same land surface model: Local-scale evaluation at an alpine site. *J. Hydrometeorol.*, **2**, 374–394.
- , and Coauthors, 2004: The Rhône-Aggregation Land Surface Scheme intercomparison project: An overview. *J. Climate*, **17**, 187–208.
- Brown, R., and R. L. Armstrong, 2008: Snow-cover data: Measurement, products, and sources. *Snow and Climate*, R. L. Armstrong and E. Brun, Eds., Cambridge University Press, 181–216.
- Brun, E., E. Martin, V. Simon, C. Gendreau, and C. Coleou, 1989: An energy and mass model of snow cover suitable for operational avalanche forecasting. *J. Glaciol.*, **35**, 333–342.
- , P. David, M. Sudul, and G. Brunot, 1992: A numerical-model to simulate snow-cover stratigraphy for operational avalanche forecasting. *J. Glaciol.*, **38**, 13–22.
- Cohen, J., M. Barlow, P. J. Kushner, and K. Saito, 2007: Stratosphere-troposphere coupling and links with Eurasian land surface variability. *J. Climate*, **20**, 5335–5343.
- Cook, B. I., G. B. Bonan, S. Levis, and H. E. Epstein, 2008: The thermoinsulation effect of snow cover within a climate model. *Climate Dyn.*, **31**, 107–124.
- Dirmeyer, P. A., A. J. Dolman, and N. Sato, 1999: The pilot phase of the Global Soil Wetness Project. *Bull. Amer. Meteor. Soc.*, **80**, 851–878.
- , X. Gao, and T. Oki, 2002: *The Second Global Soil Wetness Project Science and Implementation Plan*. International GEWEX Project Office Publication 37, 75 pp.
- Douville, H., and J. F. Royer, 1996: Sensitivity of the Asian summer monsoon to an anomalous Eurasian snow cover within the Météo-France GCM. *Climate Dyn.*, **12**, 449–466.
- , —, and J. F. Mahfouf, 1995: A new snow parameterization for the Météo-France Climate Model. 1. Validation in stand-alone experiments. *Climate Dyn.*, **12**, 21–35.
- , F. Chauvin, S. Planton, J. F. Royer, D. Salas-Melia, and S. Tyteca, 2002: Sensitivity of the hydrological cycle to increasing amounts of greenhouse gases and aerosols. *Climate Dyn.*, **20**, 45–68.
- Drusch, M., D. Vasiljevic, and P. Viterbo, 2004: ECMWF's global snow analysis: Assessment and revision based on satellite observations. *J. Appl. Meteor.*, **43**, 1282–1294.
- Dutra, E., V. M. Stepanenko, G. Balsamo, P. Viterbo, P. M. A. Miranda, D. V. Mironov, and C. Schär, 2010: An offline study of the impact of lakes on the performance of the ECMWF surface scheme. *Boreal Environ. Res.*, **15**, 100–112.
- Essery, R., and Coauthors, 2009: SNOWMIP2: An evaluation of forest snow process simulations. *Bull. Amer. Meteor. Soc.*, **90**, 1120–1135.
- Fletcher, C. G., S. C. Hardiman, P. J. Kushner, and J. Cohen, 2009: The dynamical response to snow cover perturbations in a large ensemble of atmospheric GCM integrations. *J. Climate*, **22**, 1208–1222.
- Frei, A., R. Brown, J. A. Miller, and D. A. Robinson, 2005: Snow mass over North America: Observations and results from the second phase of the atmospheric model intercomparison project. *J. Hydrometeorol.*, **6**, 681–695.
- Gao, X., P. A. Dirmeyer, and T. Oki, 2004: Update on the second global soil wetness project (GSWP-2). *GEWEX News*, Vol. 14, International GEWEX Project Office, Silver Spring, MD, 10 pp.
- Gong, G., J. Cohen, D. Entekhabi, and Y. Ge, 2007: Hemispheric-scale climate response to northern Eurasia land surface characteristics and snow anomalies. *Global Planet. Change*, **56**, 359–370.

- Grippa, M., L. Kergoat, T. Le Toan, N. M. Mognard, N. Delbart, J. L'Hermite, and S. M. Vicente-Serrano, 2005: The impact of snow depth and snowmelt on the vegetation variability over central Siberia. *Geophys. Res. Lett.*, **32**, L21412, doi:10.1029/2005GL024286.
- Groisman, P. Ya., T. R. Karl, and R. W. Knight, 1994a: Observed impact of snow cover on the heat balance and the rise of continental spring temperatures. *Science*, **263**, 198–200.
- , —, —, and G. L. Stenchikov, 1994b: Changes of snow cover, temperature, and radiative heat balance over the Northern Hemisphere. *J. Climate*, **7**, 1633–1656.
- , R. W. Knight, T. R. Karl, D. R. Easterling, B. M. Sun, and J. H. Lawrimore, 2004: Contemporary changes of the hydrological cycle over the contiguous United States: Trends derived from in situ observations. *J. Hydrometeorol.*, **5**, 64–85.
- Helfrich, S. R., D. McNamara, B. H. Ramsay, T. Baldwin, and T. Kasheta, 2007: Enhancements to, and forthcoming developments in the Interactive Multisensor Snow and Ice Mapping System (IMS). *Hydrol. Processes*, **21**, 1576–1586.
- Hirschi, M., S. I. Seneviratne, and C. Schar, 2006: Seasonal variations in terrestrial water storage for major midlatitude river basins. *J. Hydrometeorol.*, **7**, 39–60.
- Jordan, R., 1991: A one-dimensional temperature model for snow cover. CRREL Special Rep. 91-b, Cold Regions Research and Engineering Laboratory, 49 pp.
- Liu, X. D., and M. Yanai, 2002: Influence of Eurasian spring snow cover on Asian summer rainfall. *Int. J. Climatol.*, **22**, 1075–1089.
- Loth, B., H. F. Graf, and J. M. Oberhuber, 1993: Snow cover model for global climate simulations. *J. Geophys. Res.*, **98** (D6), 10 451–10 464.
- Lynch-Stieglitz, M., 1994: The development and validation of a simple snow model for the GISS GCM. *J. Climate*, **7**, 1842–1855.
- Molders, N., H. Luijting, and K. Sassen, 2008: Use of atmospheric radiation measurement program data from Barrow, Alaska, for evaluation and development of snow-albedo parameterizations. *Meteor. Atmos. Phys.*, **99**, 199–219.
- Moody, E. G., M. D. King, C. B. Schaaf, D. K. Hall, and S. Platnick, 2007: Northern Hemisphere five-year average (2000–2004) spectral albedos of surfaces in the presence of snow: Statistics computed from Terra MODIS land products. *Remote Sens. Environ.*, **111**, 337–345.
- Nijssen, B., and Coauthors, 2003: Simulation of high latitude hydrological processes in the Torne–Kalix basin: PILPS Phase 2(e): 2: Comparison of model results with observations. *Global Planet. Change*, **38**, 31–53.
- NOAA/NESDIS/OSDPD/SSD, cited 2006: IMS daily Northern Hemisphere snow and ice analysis at 4 km and 24 km resolution. National Snow and Ice Data Center, Boulder, CO, digital media. [Available online at <http://nsidc.org/data/g02156.html>.]
- Pedersen, C. A., and J. G. Winther, 2005: Intercomparison and validation of snow albedo parameterization schemes in climate models. *Climate Dyn.*, **25**, 351–362.
- Ramsay, B. H., 1998: The interactive multisensor snow and ice mapping system. *Hydrol. Processes*, **12**, 1537–1546.
- Robock, A., M. Q. Mu, K. Vinnikov, and D. Robinson, 2003: Land surface conditions over Eurasia and Indian summer monsoon rainfall. *J. Geophys. Res.*, **108**, 4131, doi:10.1029/2002JD002286.
- Roesch, A., and E. Roeckner, 2006: Assessment of snow cover and surface albedo in the ECHAM5 general circulation model. *J. Climate*, **19**, 3828–3843.
- Román, M. O., and Coauthors, 2009: The MODIS (Collection V005) BRDF/albedo product: Assessment of spatial representativeness over forested landscapes. *Remote Sens. Environ.*, **113**, 2476–2498.
- Rutter, N., D. Cline, and L. Li, 2008: Evaluation of the NOHRSC snow model (NSM) in a one-dimensional mode. *J. Hydrometeorol.*, **9**, 695–711.
- , and Coauthors, 2009: Evaluation of forest snow processes models (SnowMIP2). *J. Geophys. Res.*, **114**, D06111, doi:10.1029/2008JD011063.
- Salomon, J. G., C. B. Schaaf, A. H. Strahler, F. Gao, and Y. F. Jin, 2006: Validation of the MODIS bidirectional reflectance distribution function and albedo retrievals using combined observations from the *Aqua* and *Terra* platforms. *IEEE Trans. Geosci. Remote Sens.*, **44**, 1555–1565.
- Seneviratne, S. I., P. Viterbo, D. Luthi, and C. Schar, 2004: Inferring changes in terrestrial water storage using ERA-40 reanalysis data: The Mississippi River basin. *J. Climate*, **17**, 2039–2057.
- Sheffield, J., and Coauthors, 2003: Snow process modeling in the North American Land Data Assimilation System (NLDAS): 1. Evaluation of model-simulated snow cover extent. *J. Geophys. Res.*, **108**, 8849, doi:10.1029/2002JD003274.
- Shuai, Y. M., C. B. Schaaf, A. H. Strahler, J. C. Liu, and Z. T. Jiao, 2003: Quality assessment of BRDF/albedo retrievals in MODIS operational system. *Geophys. Res. Lett.*, **35**, L05407, doi:10.1029/2007GL032568.
- Simmons, A. J., S. M. Uppala, D. Dee, and S. Kobayashi, 2007: ERA-Interim: New ECMWF reanalysis product from 1989 onwards. *ECMWF Newsletter*, Vol. 110, ECMWF, Reading, United Kingdom, 25–35.
- Slater, A. G., A. J. Pitman, and C. E. Desborough, 1998: The validation of a snow parameterization designed for use in general circulation models. *Int. J. Climatol.*, **18**, 595–617.
- Stroeve, J., J. E. Box, F. Gao, S. L. Liang, A. Nolin, and C. Schaaf, 2005: Accuracy assessment of the MODIS 16-day albedo product for snow: Comparisons with Greenland in situ measurements. *Remote Sens. Environ.*, **94**, 46–60.
- Sun, S. F., J. M. Jin, and Y. K. Xue, 1999: A simple snow-atmosphere-soil transfer model. *J. Geophys. Res.*, **104**, 19 587–19 597.
- Tribbeck, M. J., R. J. Gurney, and E. M. Morris, 2006: The radiative effect of a fir canopy on a snowpack. *J. Hydrometeorol.*, **7**, 880–895.
- Uppala, S. M., and Coauthors, 2005: The ERA-40 Re-Analysis. *Quart. J. Roy. Meteor. Soc.*, **131**, 2961–3012.
- van den Hurk, B., and P. Viterbo, 2003: The Torne–Kalix PILPS 2(e) experiment as a test bed for modifications to the ECMWF land surface scheme. *Global Planet. Change*, **38**, 165–173.
- , —, A. C. M. Beljaars, and A. K. Betts, 2000: Offline validation of the ERA-40 surface scheme. ECMWF Tech. Memo. 295, 43 pp.
- Verseghy, D. L., 1991: Class-A Canadian Land Surface Scheme for GCMS. 1. Soil model. *Int. J. Climatol.*, **11**, 111–133.
- Viterbo, P., and A. C. M. Beljaars, 1995: An improved land-surface parameterization scheme in the ECMWF model and its validation. *J. Climate*, **8**, 2716–2748.
- , and A. K. Betts, 1999: Impact on ECMWF forecasts of changes to the albedo of the boreal forests in the presence of snow. *J. Geophys. Res.*, **104**, 27 803–27 810.
- , A. Beljaars, J. F. Mahfouf, and J. Teixeira, 1999: The representation of soil moisture freezing and its impact on the stable boundary layer. *Quart. J. Roy. Meteor. Soc.*, **125**, 2401–2426.
- Yang, Z. L., R. E. Dickinson, A. Robock, and K. Y. Vinnikov, 1997: Validation of the snow submodel of the biosphere–atmosphere transfer scheme with Russian snow cover and meteorological observational data. *J. Climate*, **10**, 353–373.